RANS Simulations of a Channel Flow with a New Velocity/Pressure-Gradient Model

Svetlana V. Poroseva[1], Juan D. Colmenares Fernandez[2],
The University of New Mexico, Albuquerque, New Mexico, 87131

and

Scott M. Murman[3]
NASA Ames Research Center, Moffett Field, CA 94035

Accurate prediction of wall-bounded flows with Reynolds-averaged Navier-Stokes turbulence models requires the improved modeling of physical processes that occur in turbulent flows such as the interaction of turbulent velocity and pressure fields, turbulent diffusion, and dissipative processes. Recently, novel models for the velocity/pressure-gradient correlations through the fourth order were proposed by the authors and successfully validated against direct numerical simulation (DNS) data in wall-bounded flows without separation in *a priori* testing. In the current work, these models are implemented in transport equations for the Reynolds stresses to evaluate the model performance in a fully-developed planar channel. Other terms that need modeling in the Reynolds stress transport equations are represented in simulations by their DNS profiles to eliminate uncertainty due to modeling these terms. Problems with using DNS data as an input in simulations are highlighted. An approach to mitigate some of those problems is proposed. The computed results are compared against DNS data.

Nomenclature

U_i = mean velocity component in the *i*-direction
U = mean velocity in the streamwise direction
Π_{ij} = velocity – pressure-gradient tensor, $1/\rho\left(< p_{,j}u_i > + < p_{,i}u_j >\right)$
Φ_{ij} = pressure-strain tensor, $1/\rho\left(< pu_{i,j} > + < pu_{j,i} >\right)$
D_{ij}^P = pressure diffusion tensor, $-1/\rho\left(< pu_i >_{,j} + < pu_j >_{,i}\right)$
D_{ij}^T = turbulent diffusion tensor, $-< u_i u_j u_k >_{,k}$
P_{ij} = production tensor, $-< u_i u_k > U_{j,k} - < u_j u_k > U_{i,k}$
Err_{ij} = budget balance error in DNS data
P = production, $1/2 P_{ii}$
ε_{ij} = dissipation tensor, $2\nu < u_{i,k} u_{j,k} >$
ε = scalar dissipation, $1/2\varepsilon_{ii}$
A_{ij}^+ = term A_{ij} in a Reynolds stress transport equation normalized in viscous parameters, $A_{ij}\nu/u_\tau^4$
$f_{i,j}$ = $\partial f_i/\partial x_j$ in the Cartesian coordinates

---

[1] Assistant Professor, Mechanical Engineering, MSC01 1104, 1 UNM Albuquerque, NM, 87131-00011, AIAA Associate Fellow.
[2] Graduate Student, Mechanical Engineering, MSC01 1105, 1 UNM Albuquerque, NM, 87131-00011, AIAA Student Member.
[3] Aerospace Engineer, NASA Ames Research Center, Moffett Field, CA 94035.

δ_{ij} = Kronecker delta tensor
h = half-channel width
u_i = velocity fluctuation in the *i*-direction
u_τ = friction velocity
u, v, w = velocity fluctuations in streamwise, normal-to-wall, and spanwise directions
x, y, z = streamwise, normal-to-wall, and spanwise directions
n_i = normal vector in the *i*-direction
δ = boundary layer thickness
ν = kinematic viscosity
k = turbulent kinetic energy
p = pressure fluctuation
ρ = density
Re_τ = Reynolds number, $\delta u_\tau / \nu$
Re_t = Reynolds number,
y_+ = $y u_\tau / \nu$
y_n = distance from the wall
$<\ldots>$ = ensemble averaging
$< u_i u_j >^+$ = $< u_i u_j > / u_\tau^2$

I. Introduction

RECently, there has been renewed interest in using a Reynolds-stress turbulence model (RSTM) for high-Reynolds-number external aerodynamics[1-3]. A major impetus behind this interest is the difficulty of existing one- and two-equation models to consistently predicted separated flows. The majority of RSTMs split the velocity/pressure-gradient correlations into pressure diffusion and pressure-strain correlations, i.e.

$$-\frac{1}{\rho}\left(< p_{,j}u_i > + < p_{,i}u_j >\right) = -\frac{1}{\rho}\left(< pu_i >_{,j} + < pu_j >_{,i}\right) + \frac{1}{\rho}\left(< pu_{i,j} > + < pu_{j,i} >\right),$$

or in common shorthand notation,

$$\Pi_{ij} = D_{ij}^P + \Phi_{ij}.$$

Although it simplifies the mathematical formulation of the problem, and separates redistribution and diffusion processes, this approach introduces difficulties in modeling the separate terms. For example, the majority of models for the pressure-strain correlations are only strictly valid in homogeneous flows, and there is little support for the gradient-diffusion model for the pressure-diffusion correlations.

An integrated approach to modeling velocity/pressure-gradient (VPG) correlations through the fourth order was recently proposed in Refs. 4 and 5. These models were successfully verified in *a priori* testing against DNS data in a fully-developed planar channel flow[6] and a zero-pressure-gradient boundary layer over a flat plate[7,8]. The goal of the current research is to validate the models for second-order VPG correlations Π_{ij}:

$$\begin{aligned}
\Pi_{xx} &= -0.1D_{xx}^T + 0.02P_{xx} + P_{xy}, \\
\Pi_{xy} &= -0.5D_{xy}^T - 0.02P_{xx} - P_{xy}, \\
\Pi_{yy} &= -0.5D_{yy}^T - 0.025P_{xx} - 0.45P_{xy}, \\
\Pi_{zz} &= -0.5D_{zz}^T + 0.025P_{xx} - 0.55P_{xy}.
\end{aligned} \tag{1}$$

through simulations conducted with an RSTM model in a fully-developed planar channel flow. In (1), the positive *y*-direction is from the wall outwards, with the *y*-value at the wall being equal to zero. Simulations were conducted at the same flow conditions as DNS in Ref. 6: $Re_\tau = 392$, $u_\tau = 0.03798$, and h = 1 *m*. Results of simulations are

compared against reference data obtained from simulations where DNS data[6] represent unknown terms (herafter, RANS-DNS simulations).

II. Modeling Framework

A. Reynolds Stress Transport Equations

In a fully-developed channel flow, only three Reynolds-averaged Navier-Stokes (RANS) equations are coupled prior to modeling: the transport equations for the mean streamwise velocity component U, the shear stress $< uv >$, and the Reynolds stress $< v^2 >$ in the normal-to-the-wall direction:

$$0 = -\frac{1}{\rho}\frac{dP}{dx} - \frac{\partial < uv >}{\partial y} + \nu\frac{\partial^2 U}{\partial y \partial y}, \tag{2}$$

$$0 = - < v^2 > \frac{\partial U}{\partial y} - \frac{\partial < uv^2 >}{\partial y} - \frac{1}{\rho}\left[< v\frac{\partial p}{\partial x} > + < u\frac{\partial p}{\partial y} > \right] - 2\nu < \left[\frac{\partial u}{\partial x}\frac{\partial v}{\partial x} + \frac{\partial u}{\partial y}\frac{\partial v}{\partial y} + \frac{\partial u}{\partial z}\frac{\partial v}{\partial z} \right] > + \nu\frac{\partial^2 < uv >}{\partial y \partial y}, \tag{3}$$

$$0 = -\frac{2}{\rho} < v\frac{\partial p}{\partial y} > - \frac{\partial < v^3 >}{\partial y} - 2\nu < \left[\left(\frac{\partial v}{\partial x}\right)^2 + \left(\frac{\partial v}{\partial y}\right)^2 + \left(\frac{\partial v}{\partial z}\right)^2 \right] > + \nu\frac{\partial^2 < v^2 >}{\partial y \partial y}. \tag{4}$$

Equations for the Reynolds stresses in the streamwise and spanwise directions depend on the solution of equations (2)-(4). The solution of $< v^2 >$-equation (4) does not depend on U and $< uv >$ prior modeling, but equations (2) and (3) are interrelated and depend on the solution of (4).

In addition to the VPG correlations, terms to be modeled in (2)-(4) are those representing turbulent diffusion and dissipation.

B. State-of-the-Art Models for Turbulent Diffusion and Dissipation

Before testing the new models for VPG correlations, common choices for models of the dissipation tensor and turbulent diffusion were evaluated in a fully-developed channel flow.

Three advanced approaches to modeling the dissipation tensor were tested: the So & Yoo[12] (SY) model, Hanjalić & Jakirlić first model[13] (HJ1), and Hanjalić & Jakirlić homogeneous model[14] (HJ2). For completeness, details of these models are presented in Appendix A. The equations for these models were solved with the OpenFOAM[15] software (simpleFOAM) using DNS data[6] as input for all flow parameters except the dissipation itself. Figures 1 and 2 compare results obtained with the SY, HJ1, and HJ2 models with DNS data.

Results for the turbulent diffusion models of Daly & Harlow[10] and Hanjalić & Launder[11] are shown in Fig. 3. The model coefficient values used for the two models are 0.2 and 0.11, respectively.

From Figs. 1-3, one can infer that none of considered models for turbulent diffusion and the dissipation tensor demonstrates accurate and reliable performance required to solve equations (2)-(4) and validate models (1). This is particularly true in the buffer zone.

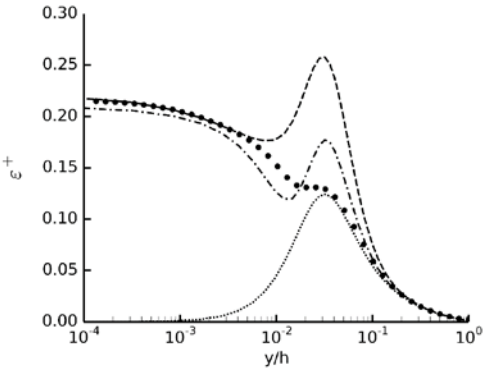

Figure 1. Scalar dissipation profiles. Notations: ⋯⋯ Eq. (A1) , − − Eq. (A2), and −·− Eq. (A4), ● ● ● DNS data[6].

C. VPG Model Validation Framework

To separate uncertainties originated from modeling turbulent diffusion and the dissipation tensor from those due to VPG correlations modeling, DNS profiles are used in the current study to represent the turbulent diffusion and dissipation terms in (2)-(4). Indeed, DNS data are considered to be the most accurate representation of a turbulent flow field obtained through computations.

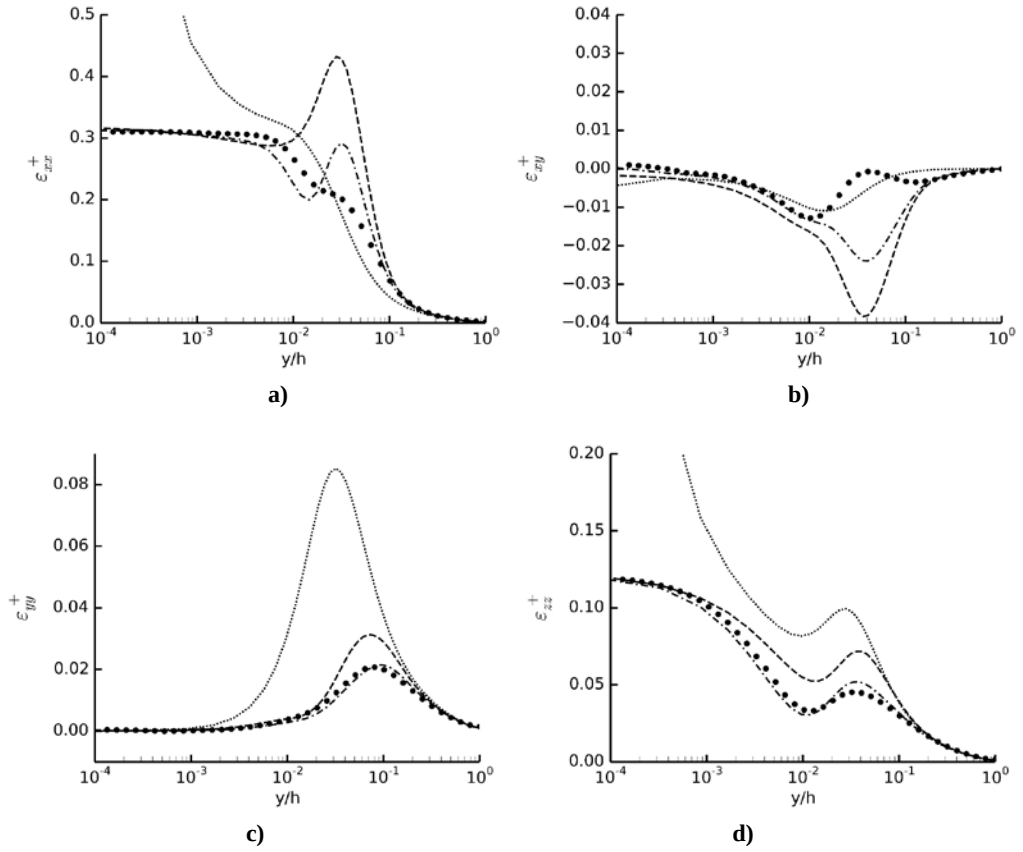

Figure 2. Turbuelnt dissipation profiles a) ε^+_{xx}, b) ε^+_{xy}, c) ε^+_{yy}, d) ε^+_{zz}. DNS data[6]: • • •. Model results: ····· So & Yoo[12], – – Hanjalić & Jakirlić[13], – · – Hanjalić & Jakirlić[14].

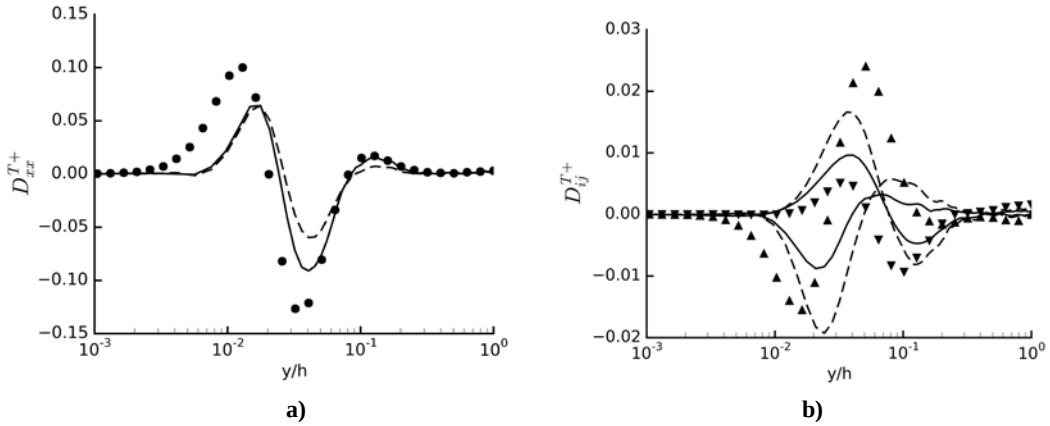

Figure 3. Turbulent diffusion profiles a) $\langle u^2 \rangle$, b) $\langle uv \rangle$ and $\langle v^2 \rangle$. DNS data[6]: • D^T_{xx}, ▲ D^T_{xy}, ▼D^T_{yy}. Model results: a) — Daly & Harlow[10], – – Hanjalić & Launder[11].

Computations are also conducted with the RST equations,

$$\frac{D<u_i u_j>}{Dt} = D_{ij}^M + D_{ij}^T + P_{ij} + \Pi_{ij} - \varepsilon_{ij} \tag{5}$$

where all terms but those corresponding to molecular diffusion are represented by DNS data (RANS-DNS simulations). Hereafter, terms in equations shown in blue are taken from DNS. This set of equations is uncoupled. Such simulations allow for quantifying uncertainty in simulations with DNS data only.

Other formulations of the RST equations solved are discussed in Section IV.

III. Numerical Approach

Two solvers are utilized in the current study: a second-order accuracy code for fully-developed axisymmetric flows and the open-source OpenFOAM software[15]. In the former, the control volume technique[16] is implemented with a pseudo-time marching scheme with time step of 0.1 s to solve parabolic equations. A grid used in simulations is non-uniform in the direction normal to the channel wall with the total number of nodes in this direction being 100 (97-node grid was used for DNS in Ref. 6). This resolution was found to be sufficient for obtaining grid-independent results. DNS profiles interpolated to the grid nodes are used as initial conditions to accelerate the results convergence. At the channel wall, non-slip boundary condition is applied to all flow parameters for which transport equations are solved. At the channel axis,

$$\frac{\partial U}{\partial y} = \frac{\partial <u_\alpha u_\alpha>}{\partial y} = <uv> = 0,$$

where $\alpha = x, y, z$ (no summation over α).

In the current study, the *simpleFoam* application from the OpenFOAM 2.3.0 library[15] is used to solve the RST equations with a Preconditioned Bi-Conjugate Gradient solver (*PBiCG*) and a Diagonal Incomplete LU (*DILU*) preconditioner. Because *simpleFoam* applies an iterative method for solving stationary problems, it uses relaxation factors to stabilize the convergence of systems of linear equations. For most applications, a relaxation factor of 0.7 guarantees stability. When solving uncoupled transport equations for the Reynolds stresses, it was found that the relaxation factor could be set to 1.0 without compromising stability of the solution. In simulations with the coupled U and $\langle uv \rangle$ equations, the relaxation factor was reduced to 0.9. Table 1 provides a list of numerical schemes used to discretize the equations.

Table 1. Numerical schemes as specified in the *fvSchemes* file.

Calculation	Keyword	Scheme
Gradient	*gradSchemes*	*Gauss linear*
Convection	*divSchemes*	*bounded Gauss linear*
Laplacian	*laplacianSchemes*	*Gauss linear corrected*
Time derivative	*timeScheme*	*steadyState*

The grid with 1×192×1 cells identical to the one from DNS[6] is used to discretize the 0.1×2×0.1 *m* domain that models the full-width of a fully-developed channel flow. Although the problem is one-dimensional, three-dimensional grids are required for use with OpenFOAM solvers. Initial values at the cell-centers are interpolated from DNS profiles[6] at the nodes using the cubic spline interpolation function from the SciPy module for Python programming language[17]. The function is a wrapper for the *splev* subroutine of the FITPACK package for FORTRAN programming language[18]. This algorithm uses lower-order (in the case of cubic splines, third-order) polynomials for various intervals and has the advantage of ensuring smooth derivatives (second derivatives for cubic splines) throughout the whole range of interpolation. Additional smoothing procedure was applied, but it did not improve the solution. Therefore, non-smoothed DNS profiles are used in the current study.

The periodic (*cyclic*) boundary condition is applied at the faces normal to the streamwise direction. Faces normal to the spanwise direction are defined as *empty*, which is a special type of boundary conditions used in OpenFOAM

for two-dimensional problems. The remaining faces are defined as the type *wall*, where non-slip boundary condition is applied to all flow parameters for which equations are solved. The pressure-gradient source term in the *U*-equation is added by specifying the *pressureGradientExplicitSource* option in the *momentumSource* dictionary, placed in the *fvOptions* OpenFOAM file inside the *system* directory of a case under consideration. To determine the pressure gradient in OpenFOAM, the bulk mean velocity is required. The mean velocity value of 0.667 is used in our study that corresponds to the bulk Reynolds number of ~13750 used in DNS[6].

Simulations with the two solvers have been conducted in parallel to minimize possible effects of errors, gids, and numerical schemes on the simulation results. Also, OpenFOAM can be used for more general flow configurations. Since similar results were obtained with both solvers, the results presented in the next section are shown without referring to the particular code they were obtained with.

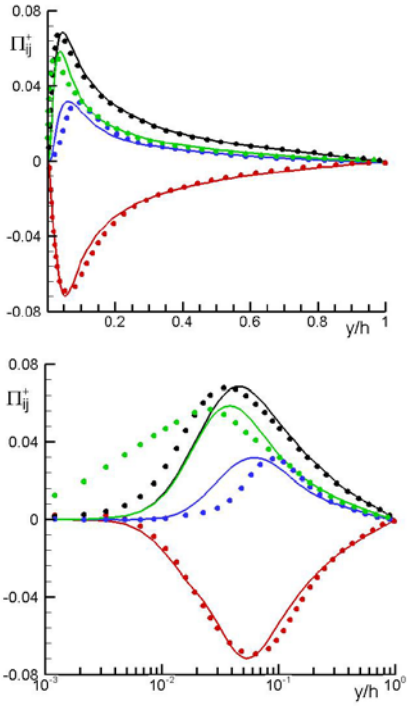

Figure 4. VPG profiles obtained from (1) using DNS data[6]. Notations: lines are models, circles are DNS data. Color: red Π_{xx}, green Π_{zz}, blue Π_{yy}, black Π_{xy}.

IV. Results and Discussion

A. A priori Testing VPG Models

Results of *a priori* testing models (1) are shown in Fig. 4 in two different scalings to demonstrate models' excellent predictive capabilities everywhere in the flow except for the very-near wall area at $y+< 10$. However, when implemented in uncoupled equations (2)-(4), with turbulent diffusion and the dissipation tensor being represented by their DNS profiles (not shown here), models produced results very off from DNS data for the Reynolds stresses. Further analysis showed that the values of model coefficients had little effect on the results. Then, to eliminate from simulations the model uncertainty, RANS-DNS simulations with equations (5) were conducted.

B. RANS-DNS Simulations

Figure 5a demonstrates a somewhat surprising result for the Reynolds stresses and the mean velocity (shown by dashed lines) obtained when solving uncoupled equations (2) and (5). In the figure, the results are compared with DNS data[6] (solid circles). Since similar results were obtained with the two different solvers used in the study, this points towards the DNS data as a major source of discrepancy between DNS and RANS-DNS simulation results.

Further analysis showed that inaccuracies in the *U*- and $< uv >$-profiles are self-mitigated when the equations for these two parameters are weakly coupled, that is, when the terms $\partial < uv > / \partial y$ in (2) and $\partial U / \partial y$ in (3) are computed, but $< v^2 >$ in the production term of (3) is taken from DNS:

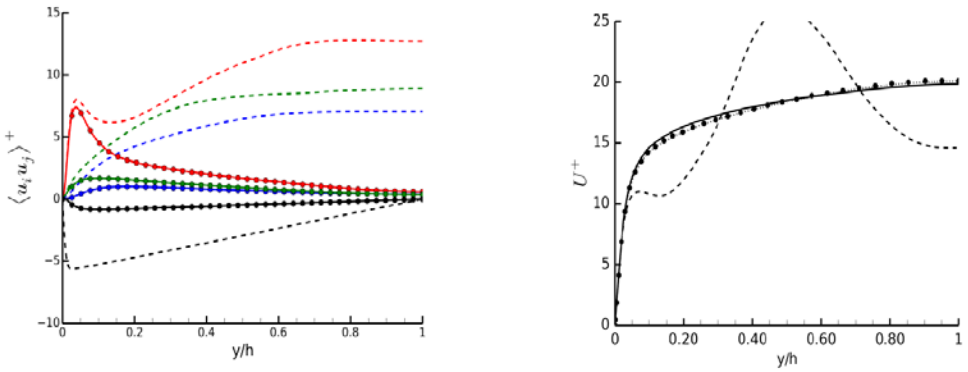

a) **b)**

Figure 5. RANS-DNS profiles: a) Reynolds stresses, b) mean velocity. Symbols: DNS data[6]. Dashed lines: uncoupled solutions with Reynolds stresses obtained from (5). Solid lines: a) Eqs. (7), b) coupled Eqs. (2) and (7). The dotted line in b): coupled Eqs. (2) and (6). Color scheme in a): red $< u^2 >^+$, green $< w^2 >^+$, blue $< v^2 >^+$, and black $< uv >^+$.

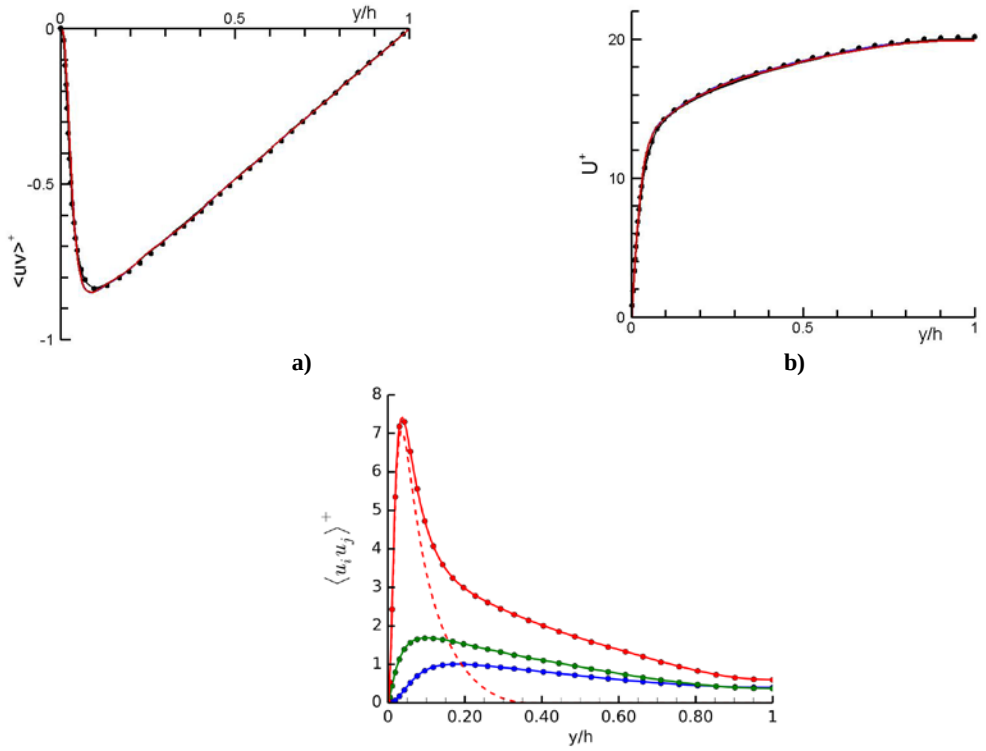

a) b) c)

Figure 6. Profiles a) $\langle uv \rangle$, b) U, c) normal Reynolds stresses. Notations: • • • DNS data[6]; a) and b) — coupled Eqs. (2) and (8); — weakly coupled Eqs. (2) and (12) for $< uv >$ with $< v^2 >$ from DNS and model (12) for Π_{xy}; c) — uncoupled Eqs. (7), − − coupled Eqs. (2) and (12) with colors as in Fig. 5a.

$$\frac{D < uv >}{Dt} = D_{xy}^{(M)} + D_{xy}^{(T)} - < v^2 > \frac{\partial U}{\partial y} + \Pi_{xy} - \varepsilon_{xy} \,. \tag{6}$$

The solution for the weakly coupled $U - < uv >$ equations is shown by black solid lines in Fig. 5 and is in agreement with DNS data[6].

The only way to correct results for the normal Reynolds stresses was found to be by incorporating the DNS balance errors as a source term in the transport equations:

$$\frac{D < u_i u_j >}{Dt} = D_{ij}^{M} + D_{ij}^{T} + P_{ij} + \Pi_{ij} - \varepsilon_{ij} - Err_{ij} \,. \tag{7}$$

This confirms that the DNS data accuracy is the major source of the observed discrepancy between the results of RANS-DNS simulations and DNS shown in Fig. 5. Indeed, closer analysis of DNS data[6] reveales that the balance errors are of the same order of magnitude or large than the molecular diffusion terms (and in some cases, other terms) particularly in the proximity of the channel axis. As such, they cannot be ignored in simulations. In Figure 5a, solutions of (7) are shown by solid lines. Clearly, the effect of inclusion of the balance errors is dramatic.

Notice that to obtain $< w^2 >$ in agreement with DNS data as shown in Fig. 5a, an additional term has to be included in Err_{zz}, the production term P_{zz}. Strictly speaking, this term should be zero in a planar flow. As small as it may appear in the DNS database[6], the production term turned out to have a strong impact on the results and thus, had to be included.

Adding the balance error to the $< uv >$-equation also improves the result for this moment when the equation is solved independently from others. However, no significant effect is observed when solving the coupled $U - < uv >$ equations, with the $< uv >$-profile obtained from (7) being in agreement with the one obtained from (6) (Fig. 5).

With the balance errors added to the RST equations, the solution of the coupled $U-<uv>-<v^2>-<u^2>$ equations

$$\frac{D<u_i u_j>}{Dt} = D_{ij}^M + D_{ij}^T + P_{ij} + \Pi_{ij} - \varepsilon_{ij} - Err_{ij}\,, \qquad (8)$$

can be obtained. (The $<w^2>$-equation in the RANS-DNS formulation is not linked to other equations by any term and thus, cannot influence or be influenced by the equations coupling.) In Figures 6a and 6b, the results are shown by black solid lines and in Fig. 6c, by dashed lines. Notice that $<v^2>$ is not affected by the equations coupling, but has an impact on U and $<uv>$ (Eqs. (2)-(4)).

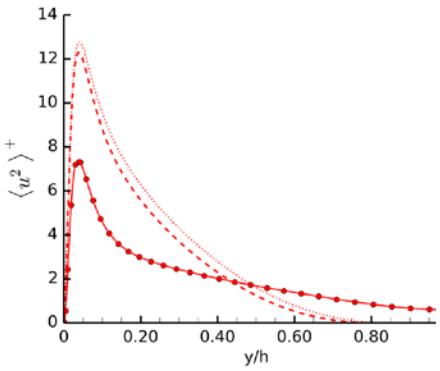

Figure 7. The $\langle u^2 \rangle$-profile from (7) with different P_{xx}. Notations: • • • DNS data[6], solid line: P_{xx} from DNS, dashed line: $\langle uv \rangle$ and $\partial U/\partial y$ from DNS, dotted line: $\langle uv \rangle$ and U from DNS, $\partial U/\partial y$ calculated.

Overall, RANS-DNS results for the coupled equations are in a good agreement with DNS data[6] for U, $<uv>$, and $<v^2>$ and thus, can be used as a reference when testing models for different terms. However, the solution for $<u^2>$ obtained with (2) and (8) (dashed line in Fig. 6c) is unphysical. Detailed analysis reveals that there is an issue associated with the production term in the transport equation for this moment. Figure 7 shows how the $<u^2>$-profile varies when solving Eq. (7) with i) P_{xx} from DNS (solid line), ii) P_{xx} calculated from $P_{xx} = -2<uv>dU/dy$ with $<uv>$ and dU/dy from DNS (dashed line), and iii) P_{xx} calculated from $P_{xx} = -2<uv>dU/dy$ with $<uv>$ and U from DNS computing dU/dy (dotted line). Clearly that the production term calculation is an error source, which is further illustrated by Fig. 8 where the P_{xx}-profiles used to obtain the results in Fig. 7 are shown.

Investigation of a possible cause of the discrepancy in P_{xx}-profiles eliminates numerical procedures from consideration, because similar results are obtained with both codes used in the current study. This leads us to assume inconsistency in DNS budgets. The error is small enough to be acceptable when confirming main terms in VPG models in *a priori* testing, but large enough to severely influence simulations. Thus, evaluation of the Π_{xx} - model through RANS-DNS simulations has to be postponed until the matter is clarified. Uncertainty associated with P_{xx} also influences the simulation results with VPG models that include this term.

C. Models Validation

Currently, all of models (1) depend on the P_{xx}-term. However, with simulations being more sensitive to the coefficients values than *a priori* testing, more accurate model formulation can be achieved.

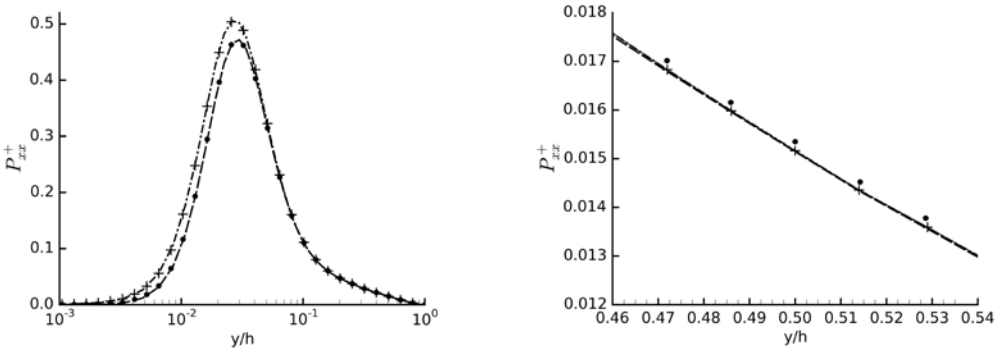

a) **b)**

Figure 8. The P_{xx} profile: a) full channel log-scale, b) zoomed in views. • DNS data[6]; + $\langle uv \rangle$ and $\partial U/\partial y$ from DNS; $-\cdot-$ $\langle uv \rangle$ and U from DNS, $\partial U/\partial y$ calculated; $--$ profile from $\langle uv \rangle$ and U coupled equations.

In particular, incorporating model (1) for Π_{xy} in equation (3) and conducting simulations of this equation coupled with *U*-equation (2) and $< v^2 >$-equation (7) (with no modeling in the latter) resulted in the model improvement:

$$\Pi_{xy} = -0.92 D_{xy}^T - 0.92 P_{xy}, \tag{9}$$

which is free from P_{xx}. The results obtained with model (9) are shown in Figs. 6a and 6b as red lines. The friction velocity value $u_\tau = 0.03798$ obtained in simulations with this model agrees with the DNS value[6]. The superior performance of model (9) to compare with model (1) for this correlation is also confirmed in *a priori* testing with DNS data used for the production and turbulent diffusion terms (Fig. 9). However, model (9) similar to model (1) does not describe the very-near wall area, which is the viscous sublayer: $y/h < 0.011$ or $y^+ \le 5$.

Simulations conducted with uncoupled equations

$$\frac{D < u_i u_j >}{Dt} = D_{ij}^M + D_{ij}^T + P_{ij} + \Pi_{ij} - \varepsilon_{ij} - Err_{ij},$$

for other Reynolds stresses revealed that the dependence of models (1) on P_{xx} for other VPG correlations cannot be eliminated.

The production term P_{xx} is not the only error source linked to DNS data in RANS-DNS simulations. Another, previously mentioned source is the production term in the $< w^2 >$-budget. An additional influential source of uncertainty in RANS-DNS simulations with VPG correlations models was found to be non-smoothness of DNS data for turbulent diffusion terms. A zoomed-in view of the problem area is shown in Fig. 10.

Whereas the DNS data accuracy should be improved prior using the RANS-DNS framework as a reliable tool for models validation, sources of deficiency of models (1) in the very-near- and near-wall areas (viscous sub-layer and buffer zone) (Fig. 4) were identified as well in the current study. A combined effort of simulations with *a priori* testing resulted in linear model expressions for all correlations but $< w^2 >$ (currently in the process) that are capable to describe the VPG correlations behavior up to the wall.

The model for Π_{xy} requires the least modifications:

$$\Pi_{xy} = -0.92 D_{xy}^T - 0.92 P_{xy} - 0.3 D_{xy}^M. \tag{10}$$

A priori solution obtained with (10) using DNS data is shown in Fig. 9 (dashed blue line). It was also found that the solution of coupled equations (2), (3), and (7) (with $< v^2 >$ from DNS) is the least sensitive to this modification, with noticeable, but rather a minor effect on *U* and $< uv >$.

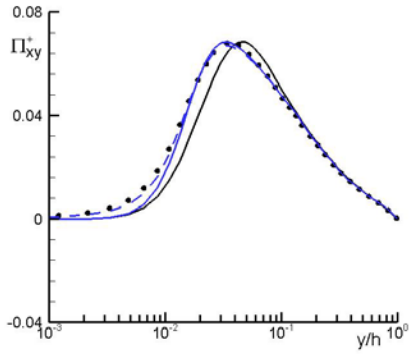

Figure 9. Results of *a priori* testing the Π_{xy} -models using DNS data[6]: — (1), — (9), – – (10). Symbols: DNS data[6].

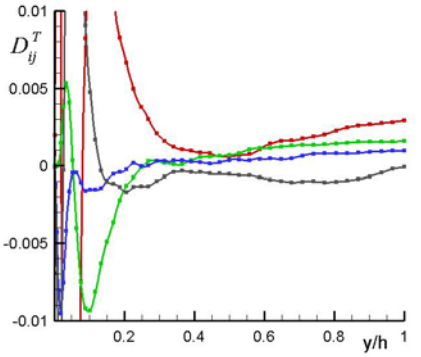

Figure 10. Zoomed-in DNS profiles[6] of turbulent diffusion terms in the RST equations. Colors as in Fig. 5a.

The best result for Π_{xx} can be obtained when this correlation is modeled as a fnction of Π_{xy} and Π_{yy}:

$$\Pi_{xx} = -0.78 \Pi_{xy} - 0.7 \Pi_{yy} - 0.25 D_{xy}^T + 0.01 D_{xx}^M. \tag{11}$$

Notice the contribution of D_{xy}^T and D_{xx}^M in this expression. Results are shown in Fig. 11.

To improve the performance of Π_{yy}-model, a more complicated contribution of the turbulent diffusion terms is required:

$$\Pi_{yy} = -0.45P_{xy} - 0.031P_{xx} - 1.35D^T_{yy} + 1.15D^T_{zz} - 0.47D^T_{xy} + 0.2D^M_{yy}, \quad (12)$$

which can be explaind by the strong wall effect on this correlation. Results of a priori testing (12) are shown in Fig. 11. Simulations with model (12) are possible, but since this model includes P_{xx} and three turbulent diffusion terms, the combined effect of DNS data uncertainties on the solution is of current concern. Testing with different DNS databases is necessary for more accurate identification of model coefficients in (10)-(12) and for more reliable computational validation of VPG models.

V. Conclusion

DNS data are currently considered as the most accurate representation of a turbulent flow field and have been used in the current study for developing and calibrating novel VPG correlations models as well as for representing turbulent diffusion and the dissipation tensor in RANS simulations to validate the developed VPG correlations models.

The previously developed VPG models for Π_{xy}, Π_{yy}, and Π_{xx} were enhanced with very-near wall predictive capabilities, that is, including the viscous sublayer flow area. In particular, it was found that a very near-wall behavior of VPG correlations can be described using molecular diffusion terms. The accurate description of the buffer zone in the Π_{yy}-profile requires more elaborated inclusion of three turbulent diffusion terms. The model for Π_{xx} is best represented as a function of Π_{xy}, Π_{yy}, D^T_{xy}, and D^M_{xx}.

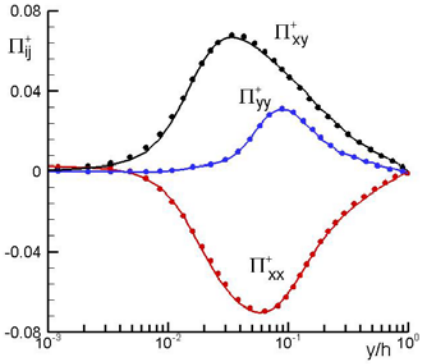

Figure 11. Results of *a priori* testing expressions (10)-(12) using DNS data[6]: — (10), — (11), — (12). Symbols: DNS data[6].

Although *a priori* testing the VPG models against DNS data resulted in an excellent agreement, RANS simulations with the developed models revealed issues associated with the DNS data accuracy used for models' calibration. Specifically, RANS simulations conducted with DNS data representing all unknown terms in transport equations, produced results that were not in agreement with DNS data for the Reynolds stresses, unless the DNS balance terms and other seemingly negligible terms from the DNS budgets were added as additional source terms in the corresponding RANS equations. Since no model can outperform DNS in principle, a more rigorous procedure than a simple estimate of the DNS budget balance errors is required.

In the paper, RANS-DNS simulations are introduced as a tool for uncertainty quantification in DNS data. The same framework can be used to quantify uncertainty associated with modeling individual physical processes and their combined effect on the simulation results. The proposed approach is the first-of-its-kind that allows for separating the model uncertainty from other uncertainty sources in simulations.

RANS simulations with the coupled equations for the mean velocity and the shear stress $< uv >$ were successful leading to the improvement of the Π_{xy}-model. However, inconsistencies and insufficient accuracy of available DNS data currently delays a progress with computing normal Reynolds stresses. The accuracy of DNS data used for models' calibration has to be addressed before models' validation through simulations can be completed.

Acknowledgments

The material is in part based upon work supported by NASA under award NNX12AJ61A and by the UNM-LANL Junior Faculty Collaborative Research Grant. A part of the simulations were conducted using the high-performance facilities at the UNM Center for Advanced Research Computing.

References

[1]Gerolymos, G.A., Lo, C., and Vallet, I., "Near-wall second moment closure based on DNS analysis of pressure correlations," AIAA Paper 2011-3574, 2011.

[2]Cécora, R.D., Eisfeld, B., Probst, A., Crippa, S. and Radespiel, R., "Differential Reynolds Stress Modeling for Aeronautics," AIAA Paper 2012-0465, 2012.

[3]Rodio, J.J., Patton, C.H., Xiao, X., and Hassan, H.A., "Simulation of the FAITH Hill Experiment using a Reynolds Stress Model," AIAA Paper 2014-2210, 2014.

[4]Poroseva, S.V., Murman, S. M., "Velocity/Pressure-Gradient Correlations in a FORANS Approach to Turbulence Modeling," AIAA2014-2207.
[5]Poroseva, S. V., Murman, S. M., "On Modelling Velocity/Pressure-Gradient Correlations in Higher-Order RANS Statistical Closures," Proc. the 19th Australasian Fluid Mechanics Conference, Melbourne, Australia, December 8-11, 2014.
[6]Jeyapaul, E., Coleman, G. N., Rumsey, C. L., "Assessment of Higher-order RANS Closures in Decelerated Planar Wall-bounded Turbulent Flow," *AIAA Aviation and Aeronautics Forum and Exposition*, Atlanta, GA, June 16-20, 2014.
[7]Sillero, J. A., Jiménez, J., Moser, R. D., 2013, "One-Point Statistics for Turbulent Wall-Bounded Flows at Reynolds Numbers up to $\delta^+ \approx 2000$," Phys. Fluids, Vol. 25, 105102 (2013); doi: 10.1063/1.4823831.
[8]Spalart, P. R., "Direct simulation of a turbulent boundary layer up to $\mathrm{Re}_\theta = 1410$," *J. Fluid Mech.*, 187, 1988, pp. 61-98.
[9]Poroseva, S. V., Murman, S. M., "Reynolds-Stress Simulations of a Fully-Developed Channel Flow Using a New Velocity/Pressure-Gradient Model," Proc. TSFP-9, Melbourne, Australia, July 1-3, 2015.
[10] Daly, B. J., Harlow, F. H., "Transport Equations in Turbulence", *Phys. Fluids*, 1970, 13, 2634-2649.
[11]Hanjalić, K. and Launder, B. E., "A Reynolds stress model of turbulence and its application to thin shear flows," *J. Fluid Mech.*, 1972, 52 (4), 609-638.
[12]So, R. M. C., and Yoo, G., "Low Reynolds Number Modeling of Turbulent Flows With and Without Wall Transpiration," *AIAA J.*, 1987, 25(12), 1556-1564.
[13]Hanjalić, K., Jakirlić, S., "A Model of Stress Dissipation in Second-Moment Closures," *Appl. Sci. Res*, 1993, 51, 513-518.
[14]Hanjalić, K., Jakirlić, S., "A New Approach to Modelling Near-Wall Turbulence Energy and Stress Dissipation," *J. Fluid Mech.*, 2002, 459, 139-166.
[15]OpenFOAM, Open-source Field Operation & Manipulation, Software Pack., Ver. 2.3.0, 2014. URL: http://www.openfoam.com/
[16]Spalding, D. B., *GENMIX: A General Computer Program for Two-Dimensional Parabolic Phenomena*, Pergamon, N, 1977.
[17]SciPy.org, "scipy.interpolate.UnivariateSpline" *Documentation*. [online] http://docs.scipy.org/doc/scipy-0.15.1/reference/generated/scipy.interpolate.UnivariateSpline.html [cited 15 May 2015].
[18]Dierckx, P., *Curve and Surface Fitting with Splines*, Monographs on numerical analysis, Oxford Univ. Press, 1995, Ch. 1.

Appendix A

In the Appendix, three models for the turbulent dissipation tested in the current study are presented. The SY (So & Yoo[12]) model includes the anisotropic model expression for the dissipation tensor:

$$\varepsilon_{ij} = \frac{2}{3}\varepsilon\delta_{ij} + 2\nu\frac{\overline{u_i' u_j'}}{y_n^2},$$

along with the equation for the scalar dissipation:

$$\frac{\partial\varepsilon}{\partial t} + U_j\frac{\partial\varepsilon}{\partial x_j} = \frac{\partial}{\partial x_k}\left[\left(\nu\delta_{lk} + c_\varepsilon\frac{\varepsilon}{k}\langle u_k u_l\rangle\right)\frac{\partial\varepsilon}{\partial x_l}\right] + \frac{\varepsilon}{k}(c_{\varepsilon 1}P - c_{\varepsilon 2}^*\varepsilon) - \frac{2\nu\varepsilon}{y_n^2}f_1 \ , \qquad \text{(A1)}$$

where $c_{\varepsilon 2}^* = c_{\varepsilon 2}\, f$, $f_1 = \exp\left(-\frac{y_n u_\tau}{2\nu}\right)$, $f = 1 - \frac{2}{9}\exp\left[-\left(\frac{Re_t}{6}\right)^2\right]$, and the model coefficients are $c_\varepsilon = 0.15, c_{\varepsilon 1} = 1.44$, and $c_{\varepsilon 2} = 1.8$. In this model, the boundary condition for the scalar dissipation is zero at the wall.

A model for the dissipation tensor in the Hanjalić & Jakirlić model[13] (HJ1) has the following form:

$$\varepsilon_{ij} = \frac{2}{3}\varepsilon\delta_{ij}(1 - f_s) + f_s\varepsilon_{ij}^*,$$

where

$$\varepsilon_{ij}^* = \frac{\varepsilon}{k}\frac{\langle u_i u_j\rangle + \left(\langle u_i u_k\rangle n_j n_k + \langle u_j u_k\rangle n_i n_k + \langle u_k u_l\rangle n_k n_l n_i n_j\right)f_d}{1 + \frac{3}{2}\frac{\langle u_p u_q\rangle}{k}n_p n_q f_d}$$

and

$$f_s = 1 - \sqrt{A}E^2,\ f_d = (1 + 0.1Re_t)^{-1},\ A = 1 - \frac{9}{8}(A_2 - A_3),\ E = 1 - \frac{9}{8}(E_2 - E_3),\ A_2 = a_{ij}a_{ji},$$

$$A_3 = a_{ij}a_{jk}a_{ki},\ a_{ij} = \frac{<u_iu_j>}{k} - \frac{2}{3}\delta_{ij},\ E_2 = e_{ij}e_{ji},\ E_3 = e_{ij}e_{jk}e_{ki},\ e_{ij} = \frac{\varepsilon_{ij}}{\varepsilon} - \frac{2}{3}\delta_{ij}.$$

The equation for the scalar dissipation in such formulation is

$$\frac{\partial \varepsilon}{\partial t} + U_j\frac{\partial \varepsilon}{\partial x_j} = \frac{\partial}{\partial x_k}\left[\left(\nu\delta_{lk} + c_\varepsilon\frac{\varepsilon}{k}\langle u_k u_l\rangle\right)\frac{\partial \varepsilon}{\partial x_l}\right] + \frac{\varepsilon}{k}(c_{\varepsilon 1}P - c^*_{\varepsilon 2}\tilde{\varepsilon}) + 2\nu\frac{k}{\varepsilon}\langle u_i u_l\rangle\left(\frac{\partial^2 U_i}{\partial x_j \partial x_l}\right)\left(\frac{\partial^2 U_i}{\partial x_k \partial x_l}\right), \tag{A2}$$

with $\tilde{\varepsilon} = \varepsilon - 2\nu\left(\frac{\partial k^{1/2}}{\partial x_n}\right)^2$, $c_\varepsilon = 0.15, c_{\varepsilon 1} = 1.44$, and $c_{\varepsilon 2} = 1.8$. The boundary condition for ε at the wall is:

$$\varepsilon_w = 2\nu\left(\frac{\partial k^{1/2}}{\partial y}\right)^2\Big|_{y=0}. \tag{A3}$$

The third formulation of a model for the dissipation tensor is the Hanjalić & Jakirlić model[14] (HJ2) with

$$\varepsilon_{ij} = \varepsilon^h_{ij} + \frac{1}{2}D^M_{ij},$$

where the dissipation tensor in homogeneous turbulence, ε^h_{ij}, is defined as

$$\varepsilon^h_{ij} = \left[\frac{2}{3}\delta_{ij}(1 - f_s) + f_s\frac{\langle u_i u_j\rangle}{k}\right]\varepsilon^h,$$

and the scalar dissipation in homogeneous turbulence is obtained by solving the following equation:

$$\begin{aligned}\frac{\partial \varepsilon^h}{\partial t} + U_j\frac{\partial \varepsilon^h}{\partial x_j} = \frac{\partial}{\partial x_k}\left[\left(\frac{1}{2}\nu\delta_{lk} + c_\varepsilon\frac{\varepsilon^h}{k}\langle u_k u_l\rangle\right)\frac{\partial \varepsilon^h}{\partial x_l}\right] + \frac{\varepsilon^h}{k}(c_{\varepsilon 1}P - c^*_{\varepsilon 2}\tilde{\varepsilon}^h)\\ - 2\nu\left[\frac{\partial\langle u_i u_k\rangle}{\partial x_l}\left(\frac{\partial^2 U_i}{\partial x_k \partial x_l}\right) + c_{\varepsilon 3}\frac{k}{\varepsilon^h}\frac{\partial\langle u_k u_l\rangle}{\partial x_j}\left(\frac{\partial U_i}{\partial x_k}\right)\left(\frac{\partial^2 U_i}{\partial x_j \partial x_l}\right)\right],\end{aligned} \tag{A4}$$

with $\tilde{\varepsilon}^h = \varepsilon^h - \nu\left(\frac{\partial k^{1/2}}{\partial x_n}\right)^2$, $c_\varepsilon = 0.18, c_{\varepsilon 1} = 1.44, c_{\varepsilon 2} = 1.8$, and $c_{\varepsilon 3} = 0.32$. Expression (A3) is used as the boundary condition for ε^h.